ARTICLE

Hierarchically Nanostructured Rutile Arrays: Acid Vapor Oxidation Growth and Tunable Morphologies

Xianfeng Yang,[†,‡] Jianle Zhuang,[†] Xiuyan Li,[†] Dihu Chen,[†] Gangfeng Ouyang,[†] Zhongquan Mao,[†] Yaxiong Han,[†] Zhenhui He,[†] Chaolun Liang, Mingmei Wu,[†,*] and Jimmy C. Yu[‡,*]

[†]MOE Key Laboratory of Bioinorganic and Synthetic Chemistry, School of Chemistry and Chemical Engineering, State Key Laboratory of Optoelectronic Materials and Technologies, School of Physics and Engineering, Instrumental Analysis and Research Centre, Sun Yat-Sen (Zhongshan) University, Guangzhou, 510275, P. R. China, and [‡]Department of Chemistry, Centre of Novel Functional Molecules, The Chinese University of Hong Kong, Shatin, Hong Kong, P. R. China

ABSTRACT A general acid vapor oxidation (AVO) strategy has been developed to grow highly oriented hierarchically structured rutile TiO_2 nanoarrays with tunable morphologies from titanium thin films. This is a simple one-pot synthesis approach involving the reaction of a titanium surface with the vapor generated from a hydrochloric acid solution in a Teflon lined autoclave. To the best of our knowledge, this is the first successful attempt to grow ordered tree-like titania nanoarrays. A possible formation mechanism for the interesting architectures has been proposed based on series of time-dependent experiments. By adjusting the initial HCl concentration, films of different rutile structures including nanotrees, dendritic nanobundles, and nanorods can be selectively obtained. Subsequently, the surface morphologies and wettability can be readily tuned.

KEYWORDS: acid vapor oxidation · film · morphology · rutile · nanotree · wettability

*Address correspondence to ceswmm@mail.sysu.edu.cn, jimyu@cuhk.edu.hk.

Received for review January 29, 2009 and accepted April 21, 2009.

Published online April 28, 2009. 10.1021/nn900084e CCC: $40.75

The assembly of one-dimensional nanobuilding blocks into orientated complex architecture is an important step in the fabrication of nanodevices.[1−4] Many complex nanostructures (such as tetrapods) of II−VI and III−V semiconductors have been prepared at high temperatures by chemical vapor deposition (CVD) and vapor−solid−liquid (VLS) methods.[5−9] During crystal growth, branched structures sometimes appear at the interface of two crystals that generally share the same lattice points (crystal twinning) at the interface.[4−10] Tree-like nanostructure arrays of II−VI and III−V semiconductors can be constructed with the assistance of initially carefully produced metal nanoclusters, which are normally left behind in the final products.[8,9] Alivisatos and Manna have proposed a method to grow tetrapoded II−VI semiconductors without using any metal catalysts.[11] Liu and Tian have developed a multiple-step growth procedure to prepare nanobranched ZnO microtree arrays in aqueous solution using initial seeds.[12−14] However, the controlled growth of new hierarchically nanostructured arrays of semiconductor compounds through a general and facile one-step route remains a major challenge.

Titanium dioxide is a typical wide-band semiconductor.[15] This versatile material has many applications including catalysts, self-cleaning (wettability), gas sensors, and photovoltaic cells.[16−22] The growth of distinctive titania films comprising one-dimensional nanostructures has received considerable research interest. A number of different techniques have been used for growing arrays of 1D titania nanostructures, such as nanowires, nanorods, and nanotubes. These include porous hard templates,[23,24] chemical deposition on a substrate by hydrolyzation of the titanium alkoxide/chloride,[21,25−27] seed-assisted growth,[28,29] electrochemically anodic oxidation[30−32] or directly thermal oxidation of a titanium metal foil (plate) in a basic aqueous solution followed by calcination at relatively high temperature (over 500 °C),[33−36] and chemical vapor deposition.[37,38] Crystalline titanium dioxide exists in nature in three polymorphs: rutile, anatase, and brookite. Rutile is the most thermodynamically stable phase. Rutile TiO_2 is generally prepared in a hydrochloride acid solution[39,40] or at high temperature calcination.[22,29,35,36] The growth of one-dimensional single crystalline rutile nanorods/nanowires in aqueous solutions has been well documented.[21,25,26,39,40] However, it has not yet been possible to directly grow hierarchical crystalline rutile nanoarrays from substrate as precursor in a facile reaction system.

The performance of a thin film is highly dependent on the surface morphology. The morphology controlled growth of a TiO_2

film structure is a key to the exploitation of features such as wettability and photocatalytic activity.[17,35,36,41] Although numerous types of TiO_2 films based on packed 0D, 1D, and/or 2D nanostructures have been reported,[21−38,41,42] the film assembled by 3D tree-like nanostructured arrays has never been described. It sounds attractive to design a general route to 1D rutile TiO_2 integrations into hierarchical 3D architecture. In this paper, we describe a simple acid vapor oxidation (AVO) method for growing hierarchical rutile TiO_2nanotree arrays without using any seeds, templates, or catalysts (Figure S1). Desirable morphologies for the film surface can be obtained by simply varying the hydrochloric acid concentration.

RESULTS AND DISCUSSION

In principle, the crystal growth of dendritic structures is generally performed in highly saturated solutions such as by VLS growth mechanism at the nucleation alloy site. However, the metal titanium that acts as both the highest saturation reactant and in situ substrate is ready to react with hot HCl aqueous solution and dissolves quickly. This is why the titanium plate is only used in nonacidic aqueous solution under thermal conditions.[28,33,34,42] In this study, a new growth approach, acid vapor oxidation (AVO) (Figure S1), was adopted to fabricate highly hierarchical nanotree arrays under facile conditions.

Figure 1 panels a and b show top- and side-view nanotree arrays grown *via* the unique AVO approach from the titanium film presputtered on a corundum plate. The "forest" is composed of uniformly oriented nanotrees rooted at the substrate. Each of the trees can reach ca. 3 μm in height and has a diameter of ca. 280 nm. The large-magnification SEM images in Figure 1 panels c and d clearly indicate an individual tree with 4-fold symmetry, which is composed of a main trunk and side nanobranches. The rough hemisphere-shaped top is formed by aligned nanobundles and/or orientated nanoparticles (the formation process is described in greater detail below).

A detailed crystallographic relationship between trunk and nanobranches was revealed by high resolution transmission electron microscopy (HRTEM), related fast-Fourier transformation (FFT), and selected area electron diffraction (SAED) along the [010] zone axis (Figure 2) and [$\bar{1}$11] zone axis (Supporting Information, Figure S2), respectively. A low magnification TEM image showed a typical individual nanotree with distinguished nanowire-like arrays atop (Figures 2a and S2a). The surfaces built up by these nanowires on the top are rough (Figure 2a and Figure S2a,b). The surface of the trunk and the side-nanobranches are also rough. Both nanowires at the top of the trunks and in the nanobranches seem to be formed by highly orientated and parallel attachment of nanoparticles, typically like those indicated by the HRTEM images as well as related

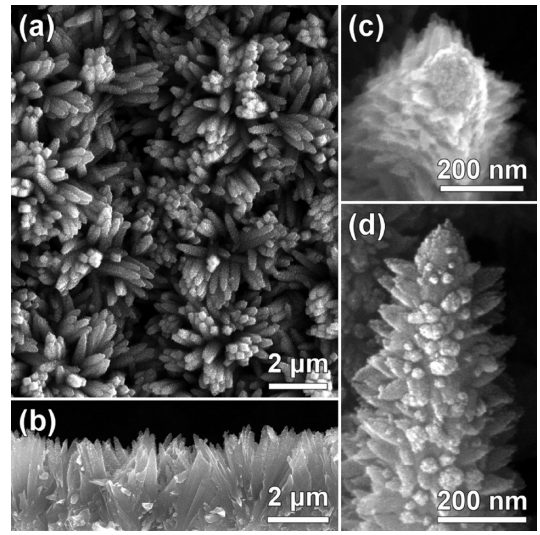

Figure 1. SEM images of branched nanotrees grown from and rooted on titanium sputtered substrate: (a, b) top and side view of a nanotree "forest", and (c, d) a typical individual nanotree.

FFT patterns (Figure S2b,d). The HRTEM image shown in Figure 2b, taken from the white square in Figure 2a, contains parts of a downward branch (square c), the trunk side (square d), and an upward branch (square e), respectively. The discontinuous lattice planes with white voids present among the lattice fringes suggest high defects in the branched nanostructures. The re-

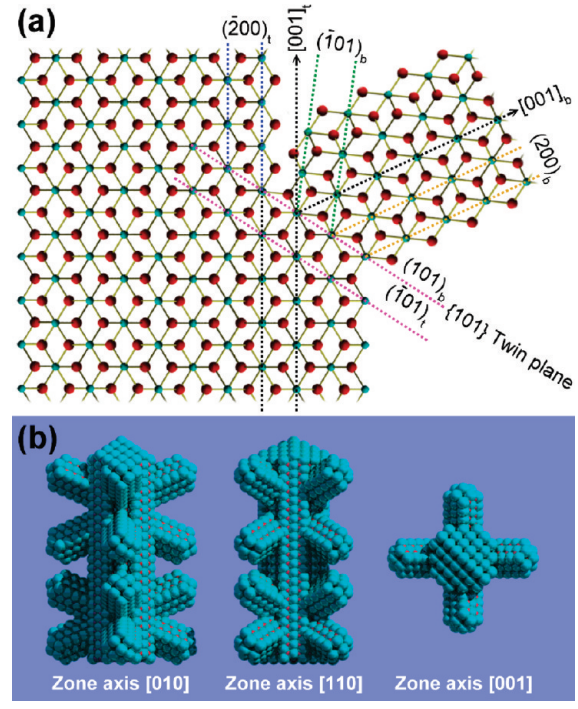

Scheme 1. (a) Schematic illustration of an atomic model sharing the equal [010] zone axes of both the trunk and the branch to highlight the coherent interface corresponding to Figure 2f in two dimensions. The blue and the red ones are representative of titanium and oxygen atoms, respectively. (b) Three-dimensional (3D) schematic illustration of atomic models along different zone axes of the trunk to clearly show the atom packing.

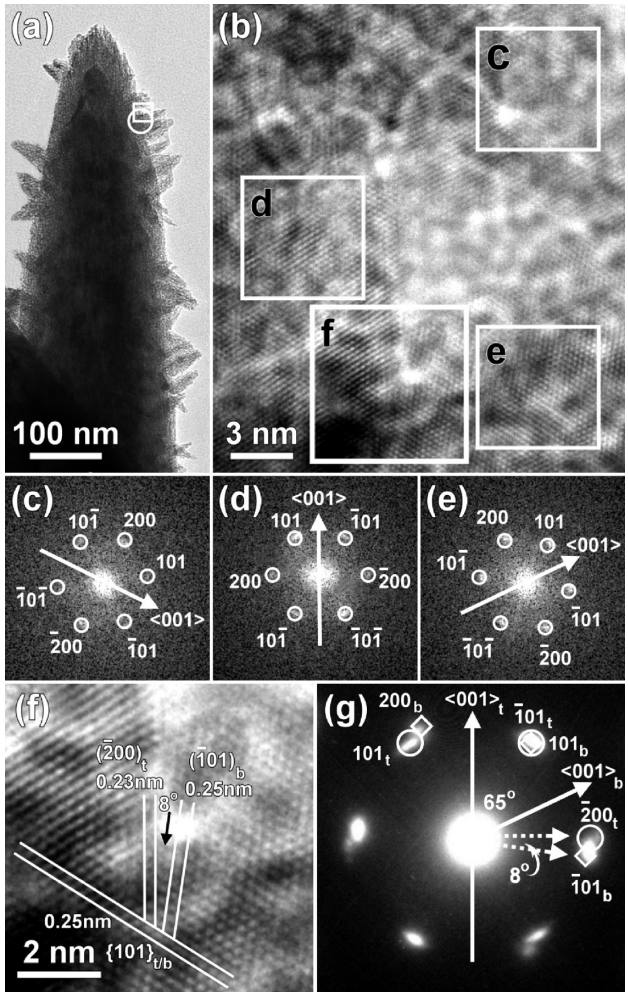

Figure 2. (a) TEM image of a branched rutile nanotree projected along the [010] zone axis. (b) HRTEM image from the area outlined by the white rectangle in panel a. (c−e) Three typical FFT patterns from the squares c, d, and e in panel b, corresponding to the areas from downward-branch (c), trunk (d), and upward-branch (e), respectively. Each white arrow indicates the growth direction of each part. (f) An enlarged HRTEM image from square f in panel b, at the connection of the trunk (denoted by subscript t) and branch (denoted by subscript b). (g) Related SAED pattern from the junction (white circle in panel a) of the trunk and upward-branch.

lated FFT patterns from white squares of c, d, and e in Figure 2b confirm that both the trunk and nanobranches are made of tetragonal rutile TiO_2 nanocrystals (JCPDS card: 78-1510, space group $P4_2/mnm$, $a = b = 0.458$ nm and $c = 0.295$ nm). The growth directions of both trunk and branches are along their *c*-axes. Relative to the trunk, there are two oblique growth directions, one downward (square c) and the other upward (square e). The SAED pattern (Figure 2g) from the white circle area in Figure 2a, associated with the enlarged HRTEM image (Figure 2f) from square f in Figure 2b, where the trunk and the upward branch connect, reveals a well established {101} twinned structure at the boundary between the trunk and the branch.[43,44] The twinned structural relationship between the trunk and a branch is shown experimentally in the HRTEM image (Figure 2f) and illustrated schematically with an atomic model in Scheme 1. The dihedral angle from planes of $(\bar{1}01)_b$ to $(\bar{2}00)_t$ and the angle from directions of $[001]_b$ to $[001]_t$ are calculated to be *ca.* 8° and 65° respectively, in principle, which accord with the experimental result (Figure 2g). The three-dimensional (3D) schematic illustrations of atomic models along [010], [110], and [001] zone axes of the trunk clearly indicate that the nanobranches are grown from the {100} side surfaces of the primary trunk and the 4-fold trunk along the *c*-axis can be considered as a {100}-trunked {110}-side-surface enclosed prism (Scheme 1b).

The growth mechanism was investigated by using a time-dependent procedure. Figure 3 shows the SEM images of the hierarchical TiO_2 nanofilms grown for a shorter and longer period: 4.0 and 12 h, respectively. When the reaction time was reduced to 4.0 h, there was a sparse growth of nanorods on the surface of the film (Figure 3a,b). At this point, only a few tiny buds formed, as the initial nucleation and growth sites of nanobranches on the rough surface and the diameter of the rods were smaller than those grown for 8.0 h (Figure 1). Up to 8.0 h, dense nanotrees were grown in arrays due to the limited space (Figure 1). When the reaction time was increased to 12 h, the nanotree increased in size overall, with some branches disappearing and others becoming bigger (Figures 3c,d). This phenomenon can be attributed to "Ostwald Ripening" just as in the growth of branched ZnO crystals as described previously.[45] Tertiary branches also appeared on the surface of the original (second) branches such as indicated by a black circle in Figure 3d. At the same time, the surfaces of both trunks and branches became smoother, but the rough hemispherical cap was still clearly observed and tended to be smoother. On the basis of the above experimental results, the following growth mechanism of the dendritic rutile TiO_2 nanotrees is proposed (Scheme 2).

First, rutile TiO_2 nanorods nucleate and grow vertically along their *c*-direction on the substrate *via* direct oxidation under HCl vapor (Scheme 2a). The initial rutile nanorods absorb titanium directly from the titanium substrate and oxygen from vapor with the assistance of HCl, just as a growing tree gains some nutrients from the ground and takes in other resources from the air. It is well-known that titanium metal reacts with hot HCl to form hydrated Ti^{3+} ions and hydrogen (Figure S3). Herein, the further oxidation and instant hydration under hot vapor can yield hydrated titania on the substrate, from which rutile seeds nucleate and nanorods grow. During the early stage of growth, longitudinal growth along ⟨001⟩ direction predominated, but at a later stage radial growth along [110] and/or [100] directions became more important, and the trunk tended to be thicker.[46,47] This 1D and 3D-combined growth might be the key aspect which causes the formation of nanobundles consisting of nanowires with orientated attachment of {110} side facets (Figure 4). The growth

of rutile nanobundles was highly favored by using a higher concentration of hydrochloric (HCl) vapor in which HCl served as both catalyst and chemical corrosive agent to favor the generation of rutile phase and to introduce defects on the rod surface, respectively. Consequently, corrosion-induced rough surfaces were formed as trunk shell and bundled nanowires were formed as the trunk core (Figure 4).

Second, twin structures were introduced in response to surface defects caused by the corrosion of the trunk surfaces by hydrochloric acid vapor. The HCl-vapor induced defects and consequently yielded {101} twins initiating the nucleation and growth of side branches from and on the {100} side surfaces (Scheme 2b) with relatively high surface energies. Third, as the aging time increased, some branches continued to grow, while a number of smaller branches disappeared, possibly because of "Ostwald Ripening" (Scheme 2c).

Fourth, HCl vapor continually plays a prominent role in the growth of one-dimensional rutile nanostructures and their side branches. With the growth of the second branches and the chemical corrosion of HCl on the sides of the branches, tertiary branches can be yielded on the initially grown and larger nanobranches at the sites previously eroded (Scheme 2d). Owing to further "Ostwald Ripening", tiny particles on the surface of the trunks and branches gradually disappeared and more smooth surfaces emerged (Figure 3c,d).

In the sequence growth of branched ZnO crystals, the use of diamine plays a prominent role in new crystal nucleation and growth on specific crystal planes by chemical erosion. The morphology and growth kinetics are remarkably dependent on the concentration of the diamine.[12−14] In this study, the use of hydrochloric acid played a crucial role in the successful growth of the hierarchical rutile nanostructure arrays. The morphology of the film surface can be varied, and surface wettability can be tuned subsequently (Figure 5). Using a lower concentration of HCl (6.0 M), a randomly orientated dendritic nanostructure is produced and the branched structures are also based on the {101} twinning (Figures S4a), which is concordant with nanotrees as described above (Figure 2). Each branch is a nanobundle; that is, it is composed of many parallel nanowires. By decreasing the concentration to 2.0 M, a large area of densely packed single crystalline nanorods grown along the ⟨001⟩ direction was fabricated (Figures S4b). The film surface formed by these nanorod arrays was much smoother than those formed by the nanotrees or dendritic nanobundles. The growth of these hierarchical nanostructures is therefore dependent on the balance of surface etching and nucleation. At a relatively high HCl concentration of 6 or 8 M, the surface etching rate is fast and many nucleation sites are generated at the initial stage. The resulting nanorods/nanowires are therefore thinner and tend to attach to each other to form bundled nanostructures. A high concentration of HCl would also etch the side surfaces of a trunk to initiate the nucleation and growth of secondary and even tertiary branches. Thus, the nanostructures of the rutile films can be tailored by altering the HCl concentration. A range of physical and chemical features, including wettability, can be modified in this way.

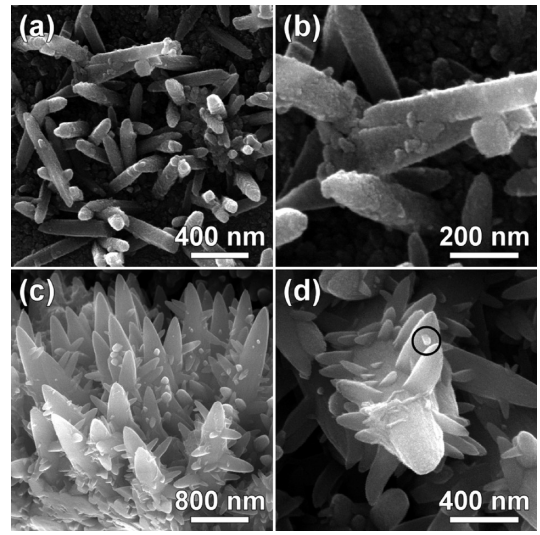

Figure 3. Time dependent growth. SEM images of the hierarchical TiO_2 nanotrees grown at different stages: (a, b) 4.0 h, (c, d) 12 h.

There is a decreasing trend of contact angle on rutile films surface from a3 to c3, as indicated by Figure 5. Besides, the surface topography changes from compact to lose as the HCl concentration increases. Meanwhile, the corresponding complexity of the hierarchical nano-building-blocks and thus film surface roughness increases. TiO_2 is an intrinsic hydrophilic material with a water contact angle of 72° and 74° on a smooth single crystal (110) and (001) surface, respec-

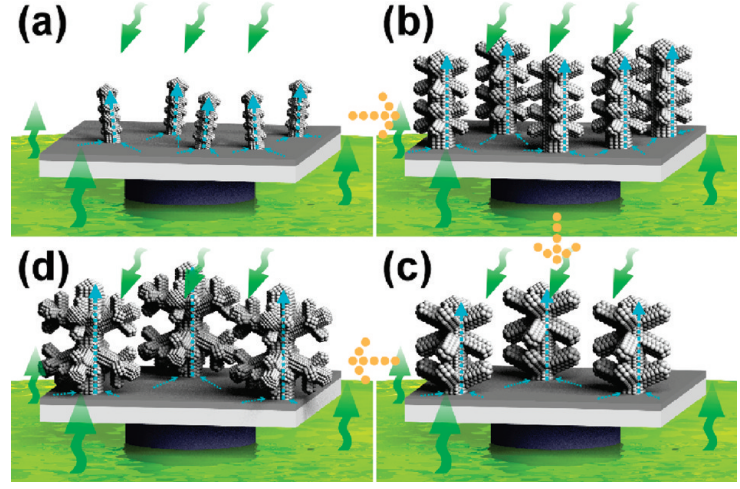

Scheme 2. Schematic illustration of the growth process: (a) no densely-distributed rodlike trunks grow from the titanium and the side surfaces are eroded; (b) obvious branches appear and the trunk tends to be more orientated due to space limitation; (c) both branches and trunks tend to be larger in dimension because of "Ostwald Ripening"; (d) ternary growth of the branches.

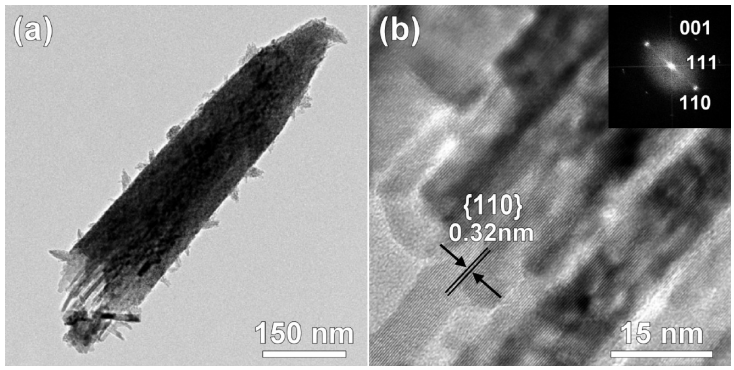

Figure 4. (a) TEM image of a transversely broken nanotree, (b) HRTEM image of the nanowires inside the nanotree with related FFT pattern (inset).

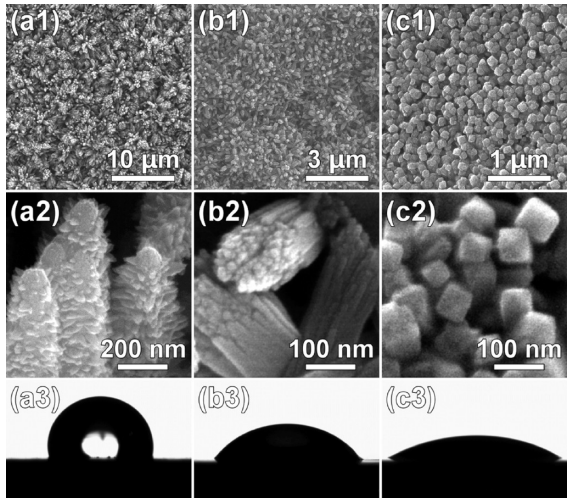

Figure 5. Low- and high-magnification SEM images of rutile films grown with HCl concentration of 8.0 (a1, a2), 6.0 (b1, b2), and 2.0 M (c1, c2). Corresponding photographs of water droplets on them (a3−c3).

tively.[25] According to the Wenzel equation, $\cos\theta^* = r\cos\theta_0$, the TiO_2 surface will be more hydrophilic when its surface becomes rough. So there is a very hydrophilic surface with contact angle of ca. 25° on the surface of Figure 5c. But with the growing of gaps, the rough surface can trap more air easily, which may cause the Wenzel contact state to become a Cassie contact state. In the Cassie equation, $\cos\theta^* = f(r\cos\theta_0 + 1) - 1$, where f is the fraction of the liquid area in contact with the solid under the droplet, suggesting that the trapped air reduces the wettability of a structured surface despite its nature.[48] Although the roughness increases, the fraction f decreases faster. As a result, the contact angle increases (Figure 5 panels b3 and a3). The film composed of nanotree arrays is especially prone to behave in a hydrophobic manner (Figure 5a3). Possibly due to this specific hierarchical structure, the water droplets on the film surface can remain in a Cassie contact state to reduce the whole system energy.

This growth methodology, a combination of *in situ* vapor oxidation and autoclaving growth, is very different from the ways in which one-dimensional titania arrays are grown in basic aqueous solution. It is also a versatile approach, since growth takes place directly on the titanium foil acting as both substrate and source, and the film morphology can also be modified (Figure S5). Hierarchical nanostructure arrays of other metal compounds such as ZnO can also be developed by using appropriate metal film or foil through this unique AVO route (Figure S6). Thus, this unique AVO method might enable a versatile approach to the growth of simple nanowire (nanorod) and complex nanotree arrays of most semiconductor compounds.

CONCLUSION

Rutile TiO_2 nanotree arrays were grown over a wide area using a one-pot facile modified autoclaving growth route defined as acid vapor oxidation (AVO). The successful growth of hierarchical nanotrees is attributed to the presence of rutile {101} twinning structure. The nanotree trunks are not a real single-crystal but possess a unique assembled nanostructure with bundled and orientated nanowires (a nanobundle) as the core and a textured nanoparticle-packed wall as the shell. These novel hierarchically structured nanoarrays might open up a new catalog of elaborate architectures for wide-band semiconductors and could have applications in the chemical, optical, and electronic fields. By varying the growth conditions, the architecture of rutile nanocrystals and surface morphologies of the films can be rationally tailored. Consequently, surface wettability can be modified. The successful fabrication of these nanostructures demonstrates the effectiveness of this new method. This novel growth strategy has considerable potential, and could readily be extended to the growth of other hierarchical semiconducting nanostructures on versatile substrates.

EXPERIMENTAL METHODS

Sample Preparation. A ceramic corundum plate (ca. 8.0 mm × 8.0 mm × 1.0 mm) was cleaned using water and acetone in an ultrasonic pool several times. Metallic Ti film with *ca.* 400 nm thickness was deposited by magnetron sputtering. This substrate was placed on a flat column positioned in the center of a Teflon cup containing a solution of hydrochloric acid as shown in Figure S1. The plate was positioned above the surface of the solution to avoid being submerged. Placed in an autoclave at 140 °C for several hours, the ceramic plate was found covered with a white surface. Precautions should be observed for the safe handling of hydrothermal reactors in which gaseous molecules may be evolved. The plate was carefully taken out from the cup, washed with distilled water, and dried in a desiccator at ambient temperature.

Characterization. The morphologies and structures of the as-prepared films were characterized by SEM (FEI Quanta 400 Thermal FE Environment scanning electron microscope) and TEM (JEOL JEM-2010HR transmission electron microscope). A dried

film for SEM observation was adhibited on the copper platform and then sputter-coated with platinum. A TEM sample was prepared by scratching tiny amounts of powder off the substrate and dispersing the powder on a holey carbon film supported on copper grids. To demonstrate morphology-related functions, the wettability of films grown under different conditions was examined. Water CAs were determined by the sessile drop method, using a Data Physics OCA20 (Germany) contact angle measuring device. The instrument provides a computer-controlled display video camera to photograph the drops, and uses an electronic syringe with 0.5 mL capacity to inject samples.

Acknowledgment. We gratefully thank Miss Lucy Antrobus from U.K. and Dr. David Wilmshurst, Academic Editor of CUHK's Research Administration Office for their fruitful discussion and revision. This work was supported financially by grants from the National Natural Science Foundation (NNSF) of China and the Government of Guangdong Province for NSF (No. U0734002, No. 50872158, and No. 8251027501000010) and industry program (No. 2006B14701002 and 2007B090400001) and China Postdoctoral Science Foundation (No. 20080440117) and a Strategic Investments Scheme administered by The Chinese University of Hong Kong.

Supporting Information Available: More electron micrographs and SAED patterns to further show the structures of the as-prepared products. This material is available free of charge *via* the Internet at http://pubs.acs.org.

REFERENCES AND NOTES

1. Lieber, C. M.; Wang, Z. L. Functional Nanowires. *MRS Bull.* **2007**, *32*, 99–108.
2. Wu, Y. Y.; Yan, H. Q.; Huang, M.; Messer, B.; Song, J. H.; Yang, P. D. Inorganic Semiconductor Nanowires: Rational Growth, Assembly, and Novel Properties. *Chem.—Eur. J.* **2002**, *8*, 1261–1268.
3. Wang, D.; Qian, F.; Yang, C.; Zhong, Z. H.; Lieber, C. M. Rational Growth of Branched and Hyperbranched Nanowire Structures. *Nano Lett.* **2004**, *4*, 871–874.
4. Wang, Z. L. *Nanowires and Nanobelts: Materials, Properties and Devices*; Kluwer Academic Publishers: Boston, MA, 2003.
5. Moore, D.; Ding, Y.; Wang, Z. L. Hierarchical Structured Nanohelices of ZnS. *Angew. Chem., Int. Ed.* **2006**, *45*, 5150–5154.
6. Hu, J. Q.; Bando, Y.; Golberg, D. Sn-Catalyzed Thermal Evaporation Synthesis of Tetrapod-Branched ZnSe Nanorod Architectures. *Small* **2005**, *1*, 95–99.
7. Gao, P. X.; Wang, Z. L. Nanopropeller Arrays of Zinc Oxide. *Appl. Phys. Lett.* **2004**, *84*, 2883–2885.
8. May, S. J.; Zheng, J. G.; Wessels, B. W.; Lauhon, L. J. Dendritic Nanowire Growth Mediated by a Self-Assembled Catalyst. *Adv. Mater.* **2005**, *17*, 598–602.
9. Dick, K. A.; Deppert, K.; Larsson, M. W.; Martensson, T.; Seifert, W.; Wallenberg, L. R.; Samuelson, L. Synthesis of Branched 'Nanotrees' by Controlled Seeding of Multiple Branching Events. *Nat. Mater.* **2004**, *3*, 380–384.
10. Ding, Y.; Wang, Z. L.; Sun, T. J.; Qiu, J. S. Zinc-Blende ZnO and Its Role in Nucleating Wurtzite Tetrapods and Twinned Nanowires. *Appl. Phys. Lett.* **2007**, *90*, 153510−1-3.
11. Manna, L.; Scher, E. C.; Alivisatos, A. P. Synthesis of Soluble and Processable Rod-, Arrow-, Teardrop-, and Tetrapod-Shaped CdSe Nanocrystals. *J. Am. Chem. Soc.* **2000**, *122*, 12700–12706.
12. Zhang, T. R.; Dong, W. J.; Keeter-Brewer, M.; Konar, S.; Njabon, R. N.; Tian, Z. R. Site-Specific Nucleation and Growth Kinetics in Hierarchical Nanosyntheses of Branched ZnO Crystallites. *J. Am. Chem. Soc.* **2006**, *128*, 10960–10968.
13. Sounart, T. L.; Liu, J.; Voigt, J. A.; Hsu, J. W. P.; Spoerke, E. D.; Tian, Z.; Jiang, Y. B. Sequential Nucleation and Growth of Complex Nanostructured Films. *Adv. Funct. Mater.* **2006**, *16*, 335–344.
14. Sounart, T. L.; Liu, J.; Voigt, J. A.; Huo, M.; Spoerke, E. D.; McKenzie, B. Secondary Nucleation and Growth of ZnO. *J. Am. Chem. Soc.* **2007**, *129*, 15786–15793.
15. Chen, X.; Mao, S. S. Titanium Dioxide Nanomaterials: Synthesis, Properties, Modifications, and Applications. *Chem. Rev.* **2007**, *107*, 2891–2959.
16. Thompson, T. L.; Yates, J. T. Surface Science Studies of the Photoactivation of TiO_2-New Photochemical Processes. *Chem. Rev.* **2006**, *106*, 4428–4453.
17. Zhang, X. T.; Jin, M.; Liu, Z. Y.; Nishimoto, S.; Saito, H.; Murakami, T.; Fujishima, A. Preparation and Photocatalytic Wettability Conversion of TiO_2-Based Superhydrophobic Surfaces. *Langmuir* **2006**, *22*, 9477–9479.
18. Li, H. X.; Bian, Z. F.; Zhu, J.; Zhang, D. Q.; Li, G. S.; Huo, Y. N.; Li, H.; Lu, Y. F. Mesoporous Titania Spheres with Tunable Chamber Structure and Enhanced Photocatalytic Activity. *J. Am. Chem. Soc.* **2007**, *129*, 8406–8413.
19. Kuang, D.; Brillet, J.; Chen, P.; Takata, M.; Uchida, S.; Miura, H.; Sumioka, K.; Zakeeruddin, S. M.; Gratzel, M. Application of Highly Ordered TiO_2 Nanotube Arrays in Flexible Dye-Sensitized Solar Cells. *ACS Nano* **2008**, *2*, 1113–1116.
20. Shankar, K.; Bandara, J.; Paulose, M.; Wietasch, H.; Varghese, O. K.; Mor, G. K.; LaTempa, T. J.; Thelakkat, M.; Grimes, C. A. Highly Efficient Solar Cells Using TiO_2 Nanotube Arrays Sensitized with a Donor-Antenna Dye. *Nano Lett.* **2008**, *8*, 1654–1659.
21. Liu, B.; Aydil, E. S. Growth of Oriented Single-Crystalline Rutile TiO_2 Nanorods on Transparent Conducting Substrates for Dye-Sensitized Solar Cells. J. Am. Chem. Soc. **2009**, *131*, 3985−3990.
22. Varghese, O. K.; Gong, D. W.; Paulose, M.; Ong, K. G.; Dickey, E. C.; Grimes, C. A. Extreme Changes in the Electrical Resistance of Titania Nanotubes with Hydrogen Exposure. *Adv. Mater.* **2003**, *15*, 624–627.
23. Sander, M. S.; Cote, M. J.; Gu, W.; Kile, B. M.; Tripp, C. P. Template-Assisted Fabrication of Dense, Aligned Arrays of Titania Nanotubes with Well-Controlled Dimensions on Substrates. *Adv. Mater.* **2004**, *16*, 2052–2057.
24. Liu, S. M.; Gan, L. M.; Liu, L. H.; Zhang, W. D.; Zeng, H. C. Synthesis of Single-Crystalline TiO_2 Nanotubes. *Chem. Mater.* **2002**, *14*, 1391–1397.
25. Feng, X. J.; Zhai, J.; Jiang, L. The Fabrication and Switchable Superhydrophobicity of TiO_2 Nanorod Films. *Angew. Chem., Int. Ed.* **2005**, *44*, 5115–5118.
26. Hosono, E.; Fujihara, S.; Kakiuchi, K.; Imai, H. Growth of Submicrometer-Scale Rectangular Parallelepiped Rutile TiO_2 Films in Aqueous $TiCl_3$ Solutions under Hydrothermal Conditions. *J. Am. Chem. Soc.* **2004**, *126*, 7790–7791.
27. Wang, D. H.; Liu, J.; Huo, Q. S.; Nie, Z. M.; Lu, W. G.; Williford, R. E.; Jiang, Y. B. Surface-Mediated Growth of Transparent, Oriented, and Well-Defined Nanocrystalline Anatase Titania Films. *J. Am. Chem. Soc.* **2006**, *128*, 13670–13671.
28. Tian, Z. R. R.; Voigt, J. A.; Liu, J.; McKenzie, B.; Xu, H. F. Large Oriented Arrays and Continuous Films of TiO_2-Based Nanotubes. *J. Am. Chem. Soc.* **2003**, *125*, 12384–12385.
29. Yoo, S.; Akbar, S. A.; Sandhage, K. H. Nanocarving of Bulk Titania Crystals into Oriented Arrays of Single-Crystal Nanofibers *via* Reaction with Hydrogen-Bearing Gas. *Adv. Mater.* **2004**, *16*, 260–264.
30. Fabregat-Santiago, F.; Barea, E. M.; Bisquert, J.; Mor, G. K.; Shankar, K.; Grimes, C. A. High Carrier Density and Capacitance in TiO_2 Nanotube Arrays Induced by Electrochemical Doping. *J. Am. Chem. Soc.* **2008**, *130*, 11312–11316.
31. Bae, S.; Kang, J.; Shim, E.; Yoon, J.; Joo, H. Correlation of Electrical and Physical Properties of Photoanode with Hydrogen Evolution in Enzymatic Photo-Electrochemical Cell. *J. Power Sources* **2008**, *179*, 863–869.
32. Cheung, K. Y.; Yip, C. T.; Djurisic, A. B.; Leung, Y. H.; Chan, W. K. Long K-Doped Titania and Titanate Nanowires on Ti Foil and Fluorine-Doped Tin Oxide/Quartz Substrates for Solar-Cell Applications. *Adv. Funct. Mater.* **2007**, *17*, 555–562.

33. Miyauchi, M.; Tokudome, H. Super-Hydrophilic and Transparent Thin Films of TiO_2 Nanotube Arrays by a Hydrothermal Reaction. *J. Mater. Chem.* **2007**, *17*, 2095–2100.
34. Peng, X. S.; Chen, A. C. Large-Scale Synthesis and Characterization of TiO_2-Based Nanostructures on Ti Substrates. *Adv. Funct. Mater.* **2006**, *16*, 1355–1362.
35. Peng, X. S.; Wang, J. P.; Thomas, D. F.; Chen, A. C. Tunable Growth of TiO_2 Nanostructures on Ti Substrates. *Nanotechnology* **2005**, *16*, 2389–2395.
36. Peng, X. S.; Chen, A. C. Aligned TiO_2 Nanorod Arrays Synthesized by Oxidizing Titanium with Acetone. *J. Mater. Chem.* **2004**, *14*, 2542–2548.
37. Wu, J. M.; Shih, H. C.; Wu, W. T. Formation and Photoluminescence of Single-Crystalline Rutile TiO_2 Nanowires Synthesized by Thermal Evaporation. *Nanotechnology* **2006**, *17*, 105–109.
38. Xiang, B.; Zhang, Y.; Wang, Z.; Luo, X. H.; Zhu, Y. W.; Zhang, H. Z.; Yu, D. P. Field-Emission Properties of TiO_2 Nanowire Arrays. *J. Phys. D, Appl. Phys.* **2005**, *38*, 1152–1155.
39. Wu, M. M.; Lin, G.; Chen, D. H.; Wang, G. G.; He, D.; Feng, S. H.; Xu, R. R. Sol-Hydrothermal Synthesis and Hydrothermally Structural Evolution of Nanocrystal Titanium Dioxide. *Chem. Mater.* **2002**, *14*, 1974–1980.
40. Li, W. J.; Shi, E. W.; Yin, Z. W. Growth Habit of Rutile and Alpha-Al_2O_3 Crystals. *J. Cryst. Growth* **2000**, *208*, 546–554.
41. O'Neill, S. A.; Parkin, I. P.; Clark, R. J. H.; Mills, A.; Elliott, N. Atmospheric Pressure Chemical Vapour Deposition of Titanium Dioxide Coatings on Glass. *J. Mater. Chem.* **2003**, *13*, 56–60.
42. Dong, W.; Zhang, T.; Epstein, J.; Cooney, L.; Wang, H.; Li, Y.; Jiang, Y. B.; Cogbill, A.; Varadan, V.; Tian, Z. R. Multifunctional Nanowire Bioscaffolds on Titanium. *Chem. Mater.* **2007**, *19*, 4454–4459.
43. Gao, Y.; Merkle, K. L.; Chang, H. L.; Zhang, T. J.; Lam, D. J. Study of Defects and Interfaces on the Atomic Scale in Epitaxial TiO_2 Thin Films on Sapphire. *Philos. Mag. A* **1992**, *65*, 1103–1125.
44. Huang, J. Y.; Park, B. H.; Jan, D.; Pan, X. Q.; Zhu, Y. T.; Jia, Q. X. High-Resolution Transmission Electron Microscopy Study of Defects and Interfaces in Epitaxial TiO_2 Films on Sapphire and $LaAlO_3$. *Philos. Mag. A* **2002**, *82*, 735–749.
45. Zhao, F. H.; Li, X. Y.; Zheng, J. G.; Yang, X. F.; Zhao, F. L.; Wong, K. S.; Wang, J.; Lin, W. J.; Wu, M. M.; Su, Q. ZnO Pine-Nanotree Arrays Grown from Facile Metal Chemical Corrosion and Oxidation. *Chem. Mater.* **2008**, *20*, 1197–1199.
46. Yang, X. F.; Konishi, H.; Xu, H. F.; Wu, M. M. Comparative Sol-Hydro(Solvo)Thermal Synthesis of TiO_2 Nanocrystals. *Eur. J. Inorg. Chem.* **2006**, 2229–2235.
47. Peng, Z. A.; Peng, X. G. Mechanisms of the Shape Evolution of CdSe Nanocrystals. *J. Am. Chem. Soc.* **2001**, *123*, 1389–1395.
48. Shiu, J. Y.; Kuo, C. W.; Chen, P. L.; Mou, C. Y. Fabrication of Tunable Superhydrophobic Surfaces by Nanosphere Lithography. *Chem. Mater.* **2004**, *16*, 561–564.